Draft version March 28, 2022
Typeset using LaTeX **twocolumn** style in AASTeX631

Improving Cosmological Parameter Measurements with a Revised Local Flow Model and Near-Infrared Supernova Observations

Erik R. Peterson[1]

[1] *Department of Physics, Duke University, Durham, NC 27708, USA*

1. INTRODUCTION

Cosmology is the study of the universe, or the *cosmos*, as a whole. In cosmology, we make a few assumptions on the state of our universe. Generally, we assume that the universe is both homogeneous and isotropic. Additionally, we model the universe as a perfect fluid. Much work at the beginning of the last century went into modeling our universe and laying the groundwork for the observations and discoveries made recently in the field of cosmology.

In the 1920s and 1930s, with Albert Einstein's newly-minted theory of general relativity, Alexander Friedmann, Georges Lemaître, Howard P. Robertson, and Arthur Geoffrey Walker each individually developed the solution to Einstein's field equations of gravitation in a homogeneous, isotropic, and expanding (or contracting) universe, now called the FLRW metric. One of the Friedmann equations, was derived using the FLRW metric,

$$\left(\frac{\ddot{a}}{a}\right) = -\frac{4\pi G}{3}\left(\rho + \frac{3p}{c^2}\right) + \frac{\Lambda c^2}{3}, \tag{1}$$

with a representing the scale factor (which governs the rate of expansion of the universe for a given time), G the gravitational constant, ρ the mass density, p the pressure, c the speed of light, and Λ the cosmological constant. There are many reasons why Eq. 1 is significant, but a direct consequence of the FLRW metric and the Friedmann equations is the development of the standard model of cosmology today, which is considered to be a flat-ΛCDM universe. Such a universe is characterized as flat, with no curvature (neither open nor closed), and consistent with a cosmological constant Λ and observations of Cold Dark Matter (CDM). The leading studies today find our universe to be composed of about 70% dark energy, 25% dark matter, and 5% baryonic matter (Planck Collaboration et al. 2020; Pantheon+: Brout et al. 2022). Given that so much of our universe seems to be composed of dark energy, which we name 'dark' energy since we cannot see it and do not know its nature, we seek to better understand how it affects our universe.

Cosmologists understood that we could better understand dark energy and better characterize our universe by observing how our universe expands (or contracts). Although Lemaître was the first to propose and present evidence for the observed cosmological relationship between distance and recession velocity for distant objects, Edwin Hubble is most recognized for the finding $v = H_0 \times d$, known now as the Hubble-Lemaître law, where the Hubble Constant H_0 is the relationship between distance d and recession velocity v and the current local rate of expansion. Cosmologists have sought to measure H_0 since then, and have done so by taking advantage of Type Ia Supernovae (SNe Ia), labeled 'standardizable candles,' by obtaining both redshifts (defined as $z = \lambda_{\rm obs}/\lambda_{\rm emit} - 1$, where λ is the wavelength observed or emitted) and brightnesses of these phenomena. Since the overall luminosity or absolute magnitude of a SN Ia is standardizable (by correcting for various empirical correlations) and given the relation,

$$\mu = m - M = 5\log\left(\frac{d}{10}\right), \tag{2}$$

We can relate apparent magnitude m with the absolute magnitude M, the difference being the distance modulus μ, to distance d in parsecs. Also by observing redshifts of these objects, we can obtain the cosmological redshifts, which can be related to the recession velocity by means of $v = z \times c$ at low redshift. Thus, with both redshifts and brightnesses, we can compare recession velocities to distances in a Hubble diagram (Fig. 1) and obtain a value for the Hubble constant H_0.

Additionally, we can better characterize our universe by measuring the dark energy equation-of-state parameter w. In ΛCDM, w ($\equiv p/\rho$) must be exactly -1 such that the pressure due to dark energy is negative (and equal in magnitude to the energy density). We can measure w by comparing relative distances of SNe and observing how well various cosmologies fit the data. Supernova cosmologists work extremely hard to measure these two important cosmological parameters, H_0 and w, well.

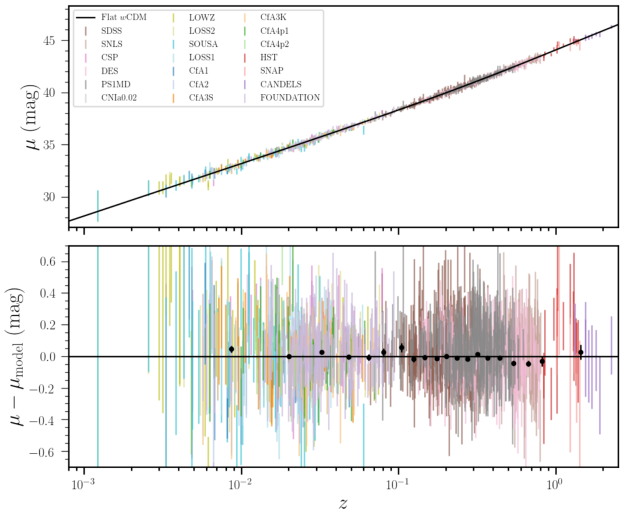

Figure 1. Hubble Diagram from Pantheon+ (Brout et al. 2022) where the distance modulus and distance modulus residuals are compared to the redshift for all 1801 SNe from all surveys. The low redshift subset of this sample is used and analyzed in my work described in later sections.

2. MODERN SUPERNOVA COSMOLOGY

Type Ia Supernovae (SNe Ia) are critical tools for measuring cosmological parameters including the Hubble constant H_0, which parameterizes the local expansion rate of the universe (Riess et al. 2016; Freedman et al. 2019), and the equation-of-state of dark energy parameter w (JLA: Betoule et al. 2014; Pantheon: Scolnic et al. 2018; DES: Brout et al. 2019). Measurements of H_0 and/or w which make use of SNe at low-redshift ($0.01 < z < 0.1$) are sensitive to the 'peculiar velocities' of host galaxies. Peculiar velocities (PVs) are the physical motions of a galaxy relative to the cosmological rest frame.

Recession velocities, $v_{\rm cosmo}$, are exactly related to cosmological redshifts $z_{\rm cosmo}$ by

$$v_{\rm cosmo} = c \int_0^{z_{\rm cosmo}} \frac{{\rm d}z}{E(z)}, \tag{3}$$

where we have used the dimensionless Hubble parameter $E(z) = H(z)/H_0$ (Harrison 1993; Peebles 1993). $z_{\rm cosmo}$ is not directly measured, but can be determined from the observed redshift corrected to the cosmic microwave background (CMB) rest frame $z_{\rm CMB}$ and the peculiar redshift approximated as $z_{\rm pec} \approx v_{\rm pec}/c$ (an approximation to the special relativistic Doppler shift) such that:

$$1 + z_{\rm cosmo} = \frac{1 + z_{\rm CMB}}{1 + z_{\rm pec}}. \tag{4}$$

The approximation $z_{\rm pec} \approx v_{\rm pec}/c$ is justified because PVs only reach ~ 600 km s^{-1}.

PVs can arise from large-scale effects due to the coherent-flow (from here on designated as CF) motion of halos such as inflow into clusters or superclusters, and smaller-scale effects due to motion within galaxy clusters. These effects overlap somewhat in scale, but larger-scale refers approximately to 10s of h^{-1} Mpc, and small scale to $< 10\ h^{-1}$ Mpc (where h is defined as $H_0/(100$ km s^{-1} Mpc$^{-1})$). We provide a descriptive graphic in Fig. 2 that explains the different components of observed galactic motion. For convenience, many analyses distinguish between motions that occur due to the masses within the volume/field of the survey being analyzed, and those due to masses beyond the extent of the survey. In total, we therefore consider four corrections applied in order to obtain better cosmological redshifts (the final three being contributions to PVs): our motion relative to the CMB rest frame, small-scale galaxy-group motion, larger-scale coherent motions, and large-scale external-field motions. These corrections are applied using

$$z_{\rm cosmo} = \left(\frac{(1 + z_{\rm observed})}{(1 + z_{\rm ecliptic})(1 + z_{\rm CMB\ dipole})(1 + z_{\rm pec})} \right) - 1 \tag{5}$$

$$z_{\rm pec} = \Big((1 + z_{\rm group})(1 + z_{\rm coh.})(1 + z_{\rm ext.\ coh.}) \Big) - 1, \tag{6}$$

which can be approximated as:

$$z_{\rm cosmo} = z_{\rm observed} - z_{\rm ecliptic} - z_{\rm CMB\ dipole} - z_{\rm pec} \tag{7}$$

$$z_{\rm pec} = z_{\rm group} + z_{\rm coh.} + z_{\rm ext.\ coh.}. \tag{8}$$

We do not use the approximated equations in this work, but they are presented here to aid the reader. The observed redshift $z_{\rm observed}$ is first corrected to the Sun's rest frame by accounting for $z_{\rm ecliptic}$ to retrieve a heliocentric redshift $z_{\rm hel}$. Next, a correction to our motion relative to the CMB dipole $z_{\rm CMB\ dipole}$ is accounted for to convert $z_{\rm hel}$ to $z_{\rm CMB}$. As shown in Eq. 4 we can obtain the cosmological redshift $z_{\rm cosmo}$ by correcting for peculiar motions. In this work those peculiar motions include: galaxy-group velocities ($v_{\rm group}$) which are motions within a group relative to the group's center of mass; CF velocities ($v_{\rm coh.}$) which are motions of groups towards large-scale attractors (e.g., Virgo); and external CF velocities ($v_{\rm ext.\ coh.}$) which are relative motions of groups towards ultra-large-scale attractors. A pictorial representation of these equations is given in Fig. 2.

PVs (~ 300 km s^{-1}) can contribute a significant fraction, up to 10%, of the overall apparent recession velocities at $z \sim 0.01$. Furthermore, PVs can be correlated

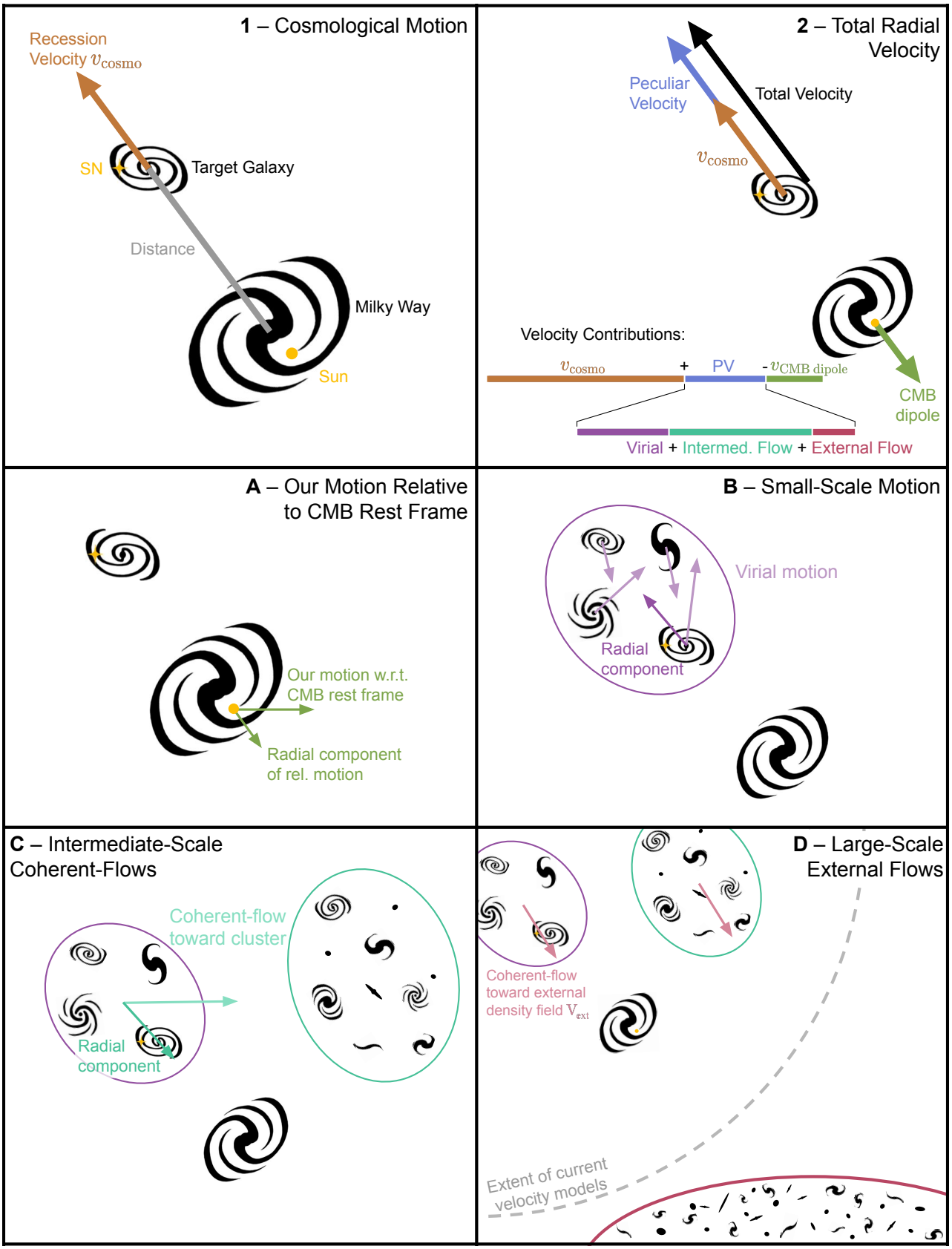

Figure 2. Explanation of the difference between the apparent cosmological motion of galaxies due to the expansion of the universe and its relation to distance (**Panel 1**) versus the observed motion of galaxies and peculiar motions (**Panel 2**). The corrections for motions are broken into four components in **Panels A-D** and include: (**A**) relative CMB motion due to the motion of our galaxy, (**B**) small-scale motions of galaxies in a group, (**C**) large-scale coherent motions of halos of galaxies moving towards each other, and (**D**) large-scale external-field motions of all galaxies moving towards a place outside the local volume of redshift surveys. All of these motions (the final three being peculiar motions) contribute a radial component to the observed motion.

across the sky and therefore may contribute systematic biases in H_0 or w (Neill et al. 2007; Conley et al. 2011). It has been widely discussed in the literature that biased redshifts at low z can propagate to significant uncertainties in the measurements of these cosmological parameters. Wojtak et al. (2015) report that a redshift bias of 10^{-4} can bias w by as much as 0.05, and similarly Calcino & Davis (2017) and Davis et al. (2019) posit that a redshift bias of 5×10^{-4} at low redshift can result in a bias of 1 km s^{-1} Mpc^{-1} in H_0.

The uncertainties in cosmological redshifts at low z come primarily from two sources: measurement uncertainty and PV uncertainty. For measurement uncertainties, these are typically on the order of $\sigma_z = 10^{-4}$. With the exception of a minority of the sample ($\sim 10\%$), the measurement uncertainties are subdominant to the PV uncertainties. Scolnic et al. (2018) derived an uncertainty in the PVs at low z of 250 km s^{-1} ($\sigma_z \approx 0.0008$) by comparing the scatter of distance modulus residuals at $z \sim 0.01$ to $z \sim 0.05$. A similar magnitude for σ_z was found in Burns et al. (2018) who solved for the PV uncertainty simultaneously in the global H_0 fit and measured uncertainties in the PVs from 200–300 km s^{-1}.

PVs to account for CFs can generally be derived in two ways. The first method is from a density field, such as 2M++ (Lavaux & Hudson 2011; Carrick et al. 2015). The PV fields depend on relations that describe how galaxies trace the total matter present. The second method for obtaining CF corrections is from distance and redshift surveys that make direct measurements on the PVs themselves, like those done by *Cosmicflows*-3 (*Cf3*; Tully et al. 2016) and the 6dF Galaxy Survey (6dF; Springob et al. 2014). The 6dF is used to construct the PV field by measuring each galaxy's distance from a fundamental plane (FP) relation and assuming that offsets from the FP are due to PVs (Springob et al. 2014).

While large CF corrections have received a significant amount of attention in the literature, corrections due to galaxy-group corrections have received less, specifically in the SN community. Galaxy groups are typically defined as associated galaxies from interdependent motion and relative distances, but the galaxy-group assignments themselves are not agreed upon in the literature. Corrections for these motions are important because they remove the small-scale velocities of galaxies relative to the group center.

While typically PVs are used in SN cosmological analyses to constrain cosmological parameters, here we test multiple sets of PVs as corrections to redshifts and observe their impact on SN cosmology. Previous works have studied several PV catalogs and methods (Boruah et al. 2020; Blakeslee et al. 2021; Rahman et al. 2021), but we aim to cover a more diverse range of catalogs here. Importantly, the analysis done here uses the same sample that is used for both Riess et al. (2021) (SH0ES) and Brout et al. (2022) and Scolnic et al. (2021) (hereafter Pantheon+).

3. DATA

We use a large compilation of low-redshift SNe from Pantheon+ to analyze various PV treatments. A full presentation of the light-curves used in this analysis (including high-z SNe) are given in Pantheon+ (Scolnic et al. 2021). In this analysis, we use the redshifts that we present in a companion paper Carr et al. (2021) who examine and re-assign the host galaxies of all the low-z SNe and query NED for the most recently acquired redshift of all the galaxies.

3.1. *Measuring Distance Modulus Values*

To measure distance modulus values for the SNe, we use `SNANA` (Kessler et al. 2009) to fit the SN light-curves with the SALT2 model (Guy et al. 2010; Betoule et al. 2014). The fits return an overall normalization x_0 related to the apparent peak brightness m_B, a stretch factor x_1, and a color parameter c for each SN. After quality cuts, in total, this low-z ($z < 0.08$) sample consists of 584 unique SNe.

To convert the fitted parameters to a distance modulus μ, we follow a modified version of the Tripp estimator (Tripp 1998) as given in Scolnic et al. (2018) where

$$\mu = m_B + \alpha x_1 - \beta c + \gamma - \Delta_B - \mathcal{M}. \quad (9)$$

Here, m_B represents the apparent peak brightness, α and β are correlation-coefficients relating x_1 and c to luminosity respectively, γ is the correction for the mass-luminosity relation (typically called the mass-step; Kelly et al. 2010; Lampeitl et al. 2010; Sullivan et al. 2010), Δ_B is the bias correction based on the BBC method using simulations (BBC method; Kessler & Scolnic 2017) and $\mathcal{M}$ is the absolute brightness of a SN with $c = 0$ and $x_1 = 0$. Following Kenworthy et al. (2019), we fix $\alpha = 0.14$ and $\beta = 3.1$, and $\gamma = 0.06$ mag such that a luminosity step of $+0.03$ mag is applied for mass $> 10^{10} M_\odot$ and -0.03 mag for mass $< 10^{10} M_\odot$.

Following Scolnic et al. (2018) we use

$$\sigma_\mu^2 = \sigma_{\rm N}^2 + \sigma_{\mu-z}^2 + \sigma_{\rm int}^2, \quad (10)$$

to calculate the total distance error (σ_μ) for the SNe in our sample by combining in quadrature: $\sigma_{\rm N}$ the measurement uncertainty of the SN distances based on m_B, x_1, and c; $\sigma_{\mu-z}$ the uncertainty from the PV uncertainty

Table 1. Group Corrections (N = 174)

Group Variant	Explanation	N (matched)
Gal	Groups not implemented	174
T15	Velocity and distance association (Tully 2015)	149
Lim17	Halo-based group finder (Lim et al. 2017)	121
Lam20	Friends of Friends algorithm (Lambert et al. 2020)	124
C07	Maximizing groups with 3 or more galaxies (Crook et al. 2007)	120

NOTE—Group acronyms are written with a short description and number of SNe matched.

and redshift measurement uncertainty; and $\sigma_{\rm int}$ the intrinsic scatter which is further discussed in section 6.1.

4. GROUP ANALYSIS

We use groups identified by Tully (2015), Lim et al. (2017), Lambert et al. (2020), and Crook et al. (2007) each individually in an attempt to calculate a group-corrected redshift, which will improve our estimate of $z_{\rm cosmo}$ by removing the motion's contribution to the observed redshift (Fig. 2.B). A summary table is given in Table 1. Tully (2015, hereafter T15) defines galaxy 'nests' or galaxy groups by associating galaxies in velocity and distance space and iteratively improving the group membership by redefining the center of the group and ensuring no overlaps occur between groups (see section 4 of T15 for details).

Lim et al. (2017, hereafter Lim17) define their groups using a halo-based group finder method, which identifies groups based on dark matter halo properties, such as mass and velocity dispersion.

Lambert et al. (2020, hereafter Lam20) implement a modified Friends of Friends algorithm (FoF; Huchra & Geller 1982) based on graph-theory with which they attempt to improve upon previous group catalogs by both keeping large clusters from being mistakenly broken down into smaller groups and avoiding the misclassification of large clusters from small groups at the same time.

Crook et al. (2007, hereafter C07) assign groups by comparing galaxy distances and velocities through a FoF algorithm. They define two galaxies to be in a group if the galaxies are within a linking distance (dependent on density) of their average redshift and their difference in redshift is within the defined linking velocity.

We match our sample of 584 SNe to their groups and determine that up to 30% (N = 174) of our low-z galaxies can be assigned to groups and note a selection bias towards the lowest redshifts due to the completeness of the catalogs used. We find that the group assignments are not biased towards a specific region in the sky. Separating the sky into four quadrants, we find that each quadrant has $28.4\% \pm 3.2\%$ of SNe found in groups.

Given these group assignments, there are a number of different options for determining the group-corrected redshift: using a simple average (Group Avg), taking the brightest galaxy's redshift (Brightest), and taking a weighted-mean (Group Mass Weight). We find the median residuals in velocity between the galaxy redshifts from each catalog and the group-averaged redshifts are on the order of 1–5 km s^{-1} (with the exception of C07) with standard deviations ranging from 200–300 km s^{-1}. For both T15 and Lim17, we obtain mass-weighted redshifts that are almost identical to the unweighted averaging.

5. COHERENT-FLOW ANALYSIS

To understand the impact of large-scale PV corrections, we obtain three sets of coherent-flow (CF) corrections for use in our analysis (Fig. 2.C, 2.D). The first set of corrections are based on 2M++ which we obtain using a velocity field reconstruction derived from the data from Lavaux & Hudson (2011). In order to extract the CF corrections from 2M++, we follow the general methodology in Carrick et al. (2015) (hereafter C15) who create a predicted PV field as a function of position in real space, and Carr et al. (2021) use that field and convert it to redshift space. We analyze a number of variations that use 2M++ data:

- 2M++ C15 — our nominal method, where the external CF model is from Carrick et al. (2015).
- 2M++$_{\rm ne}$ — similar to 2M++ C15, except 'no external' CF field is applied (i.e. $\boldsymbol{v}_{\rm ext.\ coh.} = 0$; Lavaux & Hudson 2011).
- 2M++$_{\rm ilos}$ where CF corrections are calculated by integrating over all possible distances along the line of sight. We assume a nonlinear velocity dispersion of $\sigma_v = 250$ km s^{-1} and that the PV will be normally distributed about the predicted PV.

- 2M++ [Gr] where we calculate the 2M++ CF correction at the group location (where available) rather than the individual galaxy location.
- 2M++/SDSS — similar to 2M++ C15, but applies β (the ratio of the growth rate of structure to galaxy bias $f(\Omega_m)/b$) and $v_{\text{ext. coh.}}$ determined in Said et al. (2020) from SDSS and 2M++ data.
- 2M++/SDSS$_{\text{ilos}}$ which is the same as 2M++/SDSS but integrating over all possible distances along the line of sight as in 2M++$_{\text{ilos}}$.
- 2M++/SDSS/6dF — similar to 2M++/SDSS, but using β and $v_{\text{ext. coh.}}$ determined with SDSS, 2M++, and 6dF data, as done in Said et al. (2020).

The second set of CF corrections is from *Cf3* using the methodology of forward modeling the dataset as described in Graziani et al. (2019). For the third set, we compare to a simpler model from Mould et al. (2000) who focus on CFs derived almost exclusively from the Virgo cluster, the Great Attractor, and the Shapley supercluster (hereafter VGAS). Lastly, we include a recent set from Lilow & Nusser (2021) who obtain a constrained realization of the PV field from 2MRS by utilizing both a variance-minimizing Wiener filter and random residual field realizations. We call this set of CF corrections 2MRS.

6. RESULTS

6.1. *Improvement in Hubble Residuals*

To determine the efficacy of the various PV corrections, we measure the improvement in the χ^2 and in the dispersion of the Hubble residuals about a fiducial cosmology. This is based on the assumption that removing PVs should reduce the dispersion in the Hubble diagram. We take the distance moduli (μ) and the uncertainties in the distance moduli (σ_μ) from Eq. (10) to compute Hubble residuals and a χ^2 relative to a fiducial cosmology following,

$$\Delta_{\mu,i} = \mu_{\text{obs},i} - \mu_{\text{cosmo}}(z_i) \tag{11}$$

$$\chi^2 = \sum_i \frac{\Delta^2_{\mu,i}}{\sigma^2_{\mu,i}}, \tag{12}$$

where the index i runs over all SNe in the sample, μ_{obs} is the observed distance modulus, and $\mu_{\text{cosmo}}(z)$ is the predicted distance given a redshift z and the best-fit ΛCDM parameters from the Pantheon+ analysis to calculate the distance modulus residual (Δ_μ). While we do not change the best-fit cosmology that we use to measure χ^2 when revising redshifts based on different PV analyses, we note that allowing the best-fit cosmology to vary does not alter any of the trends found. We incorporate a σ_{int} (introduced in Eq. 10) of 0.140 mag in both our group and CF analyses so that the reduced χ^2 of our distance modulus residuals is close to 1. This sets a consistent χ^2 floor for our χ^2 comparisons.

We also compute the relative standard deviation (Rel. SD), calculated by taking the median of the absolute values of Δ_μ and multiplying by 1.48 (an assumed factor for normally distributed data) for all variant redshift sets thus comparing the median absolute deviations to the standard deviation (Hoaglin et al. 2000). To be self-consistent, for both our group analysis and CF analysis, we ensure that, respectively, the same list of SNe (N = 584 for CFs and N = 174 for groups) are used among variants in the calculation. The χ^2 and Rel. SD values for each of our redshift variants are shown in Fig. 3.

6.1.1. *Group Scatter*

For our multiple methods of determining a group redshift, we compare the χ^2 of the Hubble residuals of the 174 SNe found in any of the group catalogs (Fig. 3 top left panel) to the χ^2 of the same sample when the galaxy redshifts are used. While using 2M++ C15 corrections, when we replace the galaxy redshifts with the group-averaged redshifts we find $\Delta\chi^2$ improvements of 92.5, 63.5, and 71.9 for T15, Lim17, and Lam17 respectively. We find little to no change in χ^2 ($\Delta\chi^2 < 1$) whether the group-averaged or mass-weighted method is employed. For T15 and Lim17 group corrections, averaging within the group reduces scatter compared to taking the redshift of the brightest galaxy. We find C07 to be significantly less effective at reducing scatter than corrections from all other group catalogs.

In the second panel on the left in Fig. 3, we compare the Rel. SD values obtained from our group analysis. When 2M++ C15 corrections are applied, the Rel. SD values follow the same general trend as the χ^2 values in the panel above, and differences in the trends are likely due to less sensitivity to SNe with larger magnitudes of Hubble residuals than the χ^2 calculation.

6.1.2. *Coherent-Flow Scatter*

Similarly, we measure the improvement in Hubble residuals from using the many different models for CFs: 2M++, *Cf3*, VGAS, and 2MRS from section 5 along with their variants. In the top right panel of Fig. 3, we show the χ^2 of the sample of 584 SNe when a select number of these models are used.

Using the group center to calculate the predicted CF correction (the 2M++ [Gr] variant) results in a large improvement in the scatter ($\Delta\chi^2 = -46.5$ compared to 2M++ C15 when group-corrected redshifts are not

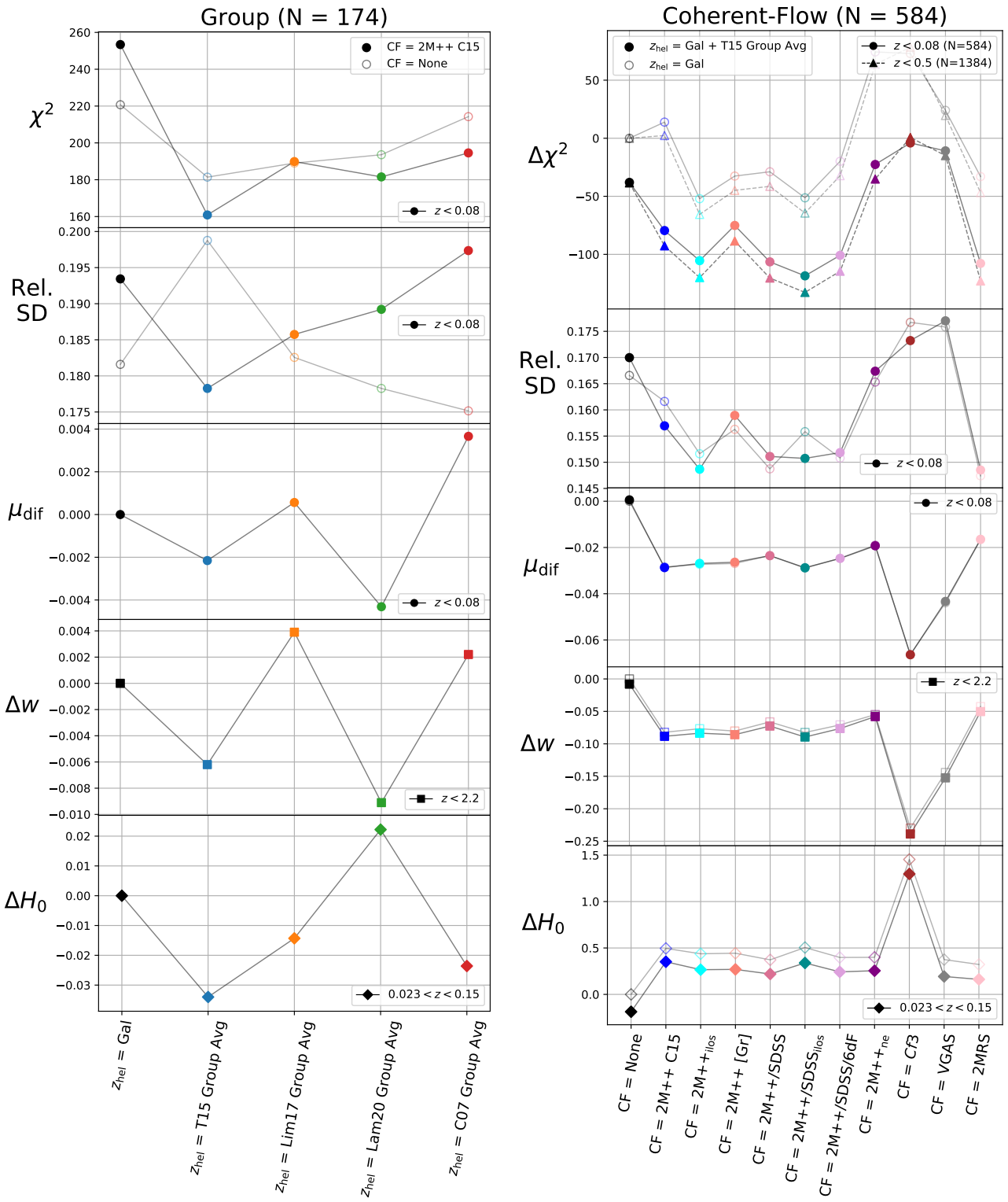

Figure 3. Results from our fitting analysis. Descriptions of all variants are provided in Table 1 and section 5. Lines are used for visualization only. **Left**: Group χ^2, relative standard deviation of the Hubble residual (Rel. SD), difference in weighted mean distance modulus residuals ($\mu_{\rm dif}$), Δw, and ΔH_0 for Tully (2015), Lim et al. (2017), Lambert et al. (2020), and Crook et al. (2007) group-averaged redshift variants as compared with the galaxy redshift variant. We compare χ^2 values with (solid points) and without (open points) an additional CF correction. In the first, second, and third panels we present values calculated by using only SNe updated as described in our group analysis (N = 174). In all panels, only SNe found in groups (N = 174) vary between points on a line with some panels showing values calculated with samples covering differing redshift ranges. The fourth and fifth panels are calculated with $z < 2.2$, and $0.023 < z < 0.15$ respectively. **Right**: Comparing $\Delta\chi^2$, Rel. SD, $\mu_{\rm dif}$, Δw, and ΔH_0 for various CF corrections applied to the individual galaxy redshifts or group-averaged heliocentric redshifts from T15, where available. Additionally plotted with open points are redshift sets with solely individual galaxy redshifts. In the first panel, the improvements in χ^2 for two upper limits of redshift are shown. Each redshift range is specified in the legends.

also included), but integrating over all possible distances along the line of sight (2M++$_{\rm ilos}$) results in an even larger improvement in scatter ($\Delta\chi^2 = -66.0$). The 2M++/SDSS, 2M++/SDSS/6dF, and 2MRS variants are similar in scatter improvement with $\Delta\chi^2$ ranging from ~ -35–45.

Furthermore, considering that we use roughly 3× as many SNe in the CF analysis as in the group analysis, it is noteworthy that none of the CFs improve the χ^2 as much as the group corrections. Similar to the group Rel. SD panel on the left, the CF Rel. SD values as seen in the right side of Fig. 3 follow the same general trend as the χ^2 values.

Additionally, we measure the impact of the CF corrections when we also include group averaging from T15 ($z_{\rm hel}$ = Gal + T15 Group Avg). As shown in the top right panel of Fig. 3, there is a large improvement in χ^2 for all variants when groups are incorporated as well. When including group-corrected redshifts, the 2M++/SDSS$_{\rm ilos}$ variant results in the largest improvement in scatter among CF corrections as compared to 2M++ C15 ($\Delta\chi^2 = -39.0$), but the overall improvement in scatter is comparable to the improvements seen from the 2M++$_{\rm ilos}$, 2M++/SDSS, 2M++/SDSS/6dF, 2MRS, and 2MRS$_{\rm ilos}$ variants. We see that while group assignment reduces the χ^2, the largest reduction is when both group corrections and CF corrections are applied.

6.2. *Impact on Measurement of Cosmological Parameters*

We define $\mu_{\rm dif}$ for each sample as the difference in the weighted mean of the low-redshift SN vector of Δ_μ (Eq. 11) with uncertainties σ_μ (Eq. 10) and plot $\mu_{\rm dif}$ in the third panels of Fig. 3. We propagate these differences in μ to a difference in both w and H_0 in the fourth and fifth panels of Fig. 3. Following Kessler & Scolnic (2017), we measure the change in w using the **wfit** program in `SNANA`, with approximate priors from Planck CMB measurements (Planck Collaboration et al. 2020) for $z < 2.2$ (high-z SNe presented in Pantheon+). To measure the change in H_0, we determine the change in the mean intercept, as shown in the bottom panel of Fig. 3, but limited to a redshift range of $0.023 < z < 0.15$ and follow the formulas outlined in Riess et al. (2016).

6.2.1. *Impact from Group Corrections*

In the third panel on the left of Fig. 3, we show the change in the mean value of the distance modulus residuals $\mu_{\rm dif}$ for all the SNe impacted by the group corrections to redshifts. We find that the impact of the group corrections is on the few mmag scale when only looking at the 174 SNe affected, which would be on the 1-mmag scale when including the full set of SNe at low z.

For w, we compare the same galaxy redshift variant to the unweighted-averaged variants using the whole redshift range from $z < 2.2$ and find $\sigma_w = 0.005$, which is again a small amount relative to the statistical uncertainty of 0.04 (fourth panel on the left of Fig. 3; Scolnic et al. 2018). As for H_0, all changes are within $\sigma_{\rm H_0} = 0.05$ km s^{-1} Mpc^{-1}, which is a negligible fraction of the uncertainty in H_0 of ~ 1.5 km s^{-1} Mpc^{-1} (fifth panel on the left of Fig. 3; Riess et al. 2019).

6.2.2. *Impact from Coherent-Flow Corrections*

We make the same assessments for the CF corrections. The third panel on the right of Fig. 3 presents the mean distance modulus residuals in comparison to the CF = None redshift variant $\mu_{\rm dif}$ for SNe with $z < 0.08$. Overall, the impact on $\mu_{\rm dif}$ is much larger for the CF corrections than the group corrections.

From the fourth and fifth panels on the right of Fig. 3, we measure a change of $\Delta w = -0.08$ and $\Delta{\rm H_0} = +0.50$ km s^{-1} Mpc^{-1} between the CF = 2M++ C15 and CF = None cases. The largest disparities are seen when using the *Cf3* and VGAS corrections, however as seen in the χ^2 and Rel. SD panels, both *Cf3* and VGAS also make the scatter worse by the largest amounts. The CF treatments that result in the greatest improvement in scatter, CF = 2M++/SDSS$_{\rm ilos}$ and CF = 2MRS, vary w by 0.04 and H_0 by 0.18 km s^{-1} Mpc^{-1}.

7. DISCUSSION

In this work, we study two corrections due to PVs for low-redshift galaxies. The first correction is due to assigning galaxies to groups. We examine multiple different methods and find a relatively similar impact. The choice of using group redshifts is clear, and the data prefers the T15 catalog, with the second best option being Lam20 which can be used as a systematic variant.

For CF corrections, we find that the 2M++ and 2MRS corrections are optimal. However, from Fig. 3, we show that in terms of reducing the χ^2, integrating over all possible distances along the line of sight and updating β and the $v_{\rm ext.\ coh.}$ according to SDSS and 2M++ data, or using the 2MRS corrections is preferred. Past analyses by SN cosmologists measuring w (Betoule et al. 2014; Scolnic et al. 2018; Brout et al. 2019) have not used these techniques. One potential explanation for the improvement observed from integrating along the line of sight is that this integration helps account for noise at small scales without removing large-scale correlations that affect the central values of w/H_0. Group corrections however remove nonlinear motions that cause large scatter at low-redshift, but have little effect on those same central values (see Fig. 2 for visualization).

8. PLAN FOR FUTURE RESEARCH

I am the lead graduate student for the Dark Energy, H_0, and peculiar Velocities using Infrared Light from Supernovae (DEHVILS) survey which is designed to tackle some of the most pressing problems in cosmology today, while laying the groundwork for the next generation of cosmological measurements. The survey aims to use SN Ia observed at near-infrared (NIR) wavelengths to improve measurements of dark energy parameters, H_0, and the growth of structure parameter $f\sigma_8$ in the nearby universe, while developing a low-z SN Ia anchor sample for the wealth of data from the Rubin Observatory and the *Roman Space Telescope* in the 2020s.

In almost every previous cosmological study with SNe Ia, SNe Ia have been measured in the optical, but it has been shown that SNe Ia observed in the near infrared (NIR) can be better standard candles, as they are less susceptible to uncertainties due to dust around the SN Ia (Burns et al. 2011).

To date, quality SN Ia light curves in the NIR are sparse. Therefore, my thesis project is to build the largest and highest quality sample of NIR light curves to improve measurements of H_0 and w. Furthermore, because my sample is focused on low redshifts, I can better constrain the growth-of-structure parameter $f\sigma_8$ and better characterize the peculiar velocity field in our nearby universe. I have three primary goals for the analysis of this dataset:

1. Understand the physics of SNe Ia in the NIR. My first analysis project with this sample will study whether the luminosity of SNe Ia in the NIR is correlated with host galaxy properties. This correlation has been seen for SN Ia brightnesses in the optical, and it is now a serious debate about whether the same thing can be found in the NIR (Uddin et al. 2020; Ponder et al. 2021). This question of whether or not a host galaxy correlation is seen in the NIR is significant because it can tell us whether or not these correlations are due to dust around the SNe (Brout & Scolnic 2021) or due to differences in progenitor systems of the SNe (e.g., Rigault et al. 2013).

2. My second goal is to measure the Hubble constant and the growth-of-structure in the nearby universe. Measurements of these values from different cosmological probes have been seen to be in tension (e.g., Riess et al. 2016; Wright et al. 2020, KiDs), though it is still unclear if this is due to new physics or systematics. My sample, by measuring distances to SNe Ia and inferring peculiar velocities, can constrain both H_0 and $f\sigma_8$ and attempt to validate the significance of these tensions as well as see if these two tensions are related.

3. My third goal is to create a legacy dataset that will serve as a systematic crosscheck for the Legacy Survey of Space and Time (LSST) and an anchor sample for *Roman*. As LSST only surveys the optical, the SN Ia survey may likely hit a systematic floor due to its modeling of SN Ia physics. A NIR sample can help LSST break this floor by allowing us to better model the intrinsic scatter of the SNe. Furthermore, *Roman* will measure NIR light curves at a redshift of 0.5 but will need a low-z sample as an anchor to produce relative distance measurements of SNe and constrain the nature of dark energy. There is no other ongoing low-z survey in the NIR, and it is critical we provide these future surveys with what they need to succeed.

My work in this project has already begun. I have already obtained light curves for 105 SNe and have begun work on analysis. Such work has involved data reduction, including the use of online templates, image subtraction (see Fig. 4), data management, host galaxy analysis, and calibration checks. I plan on submitting the DEHVILS data release (DR1) for publication by the end of this year.

Software: `SNANA` (Kessler et al. 2009), astropy (Astropy Collaboration et al. 2013; Price-Whelan et al. 2018) matplotlib (Hunter 2007), numpy (Van Der Walt et al. 2011), PIPPIN (Hinton & Brout 2020).

REFERENCES

Astropy Collaboration, Robitaille, T. P., Tollerud, E. J., et al., 2013, A&A, 558, A33, arXiv:1307.6212

Betoule, M., Kessler, R., Guy, J., et al., 2014, A&A, 568, A22, arXiv:1401.4064

Blakeslee, J. P., Jensen, J. B., Ma, C.-P., Milne, P. A., Greene, J. E., 2021, ApJ, 911, 1, 65, arXiv:2101.02221

Boruah, S. S., Hudson, M. J., Lavaux, G., 2020, arXiv e-prints, arXiv:2010.01119, arXiv:2010.01119

Brout, D., Scolnic, D., 2021, ApJ, 909, 1, 26, arXiv:2004.10206

Brout, D., Scolnic, D., Kessler, R., et al., 2019, ApJ, 874, 2, 150, arXiv:1811.02377

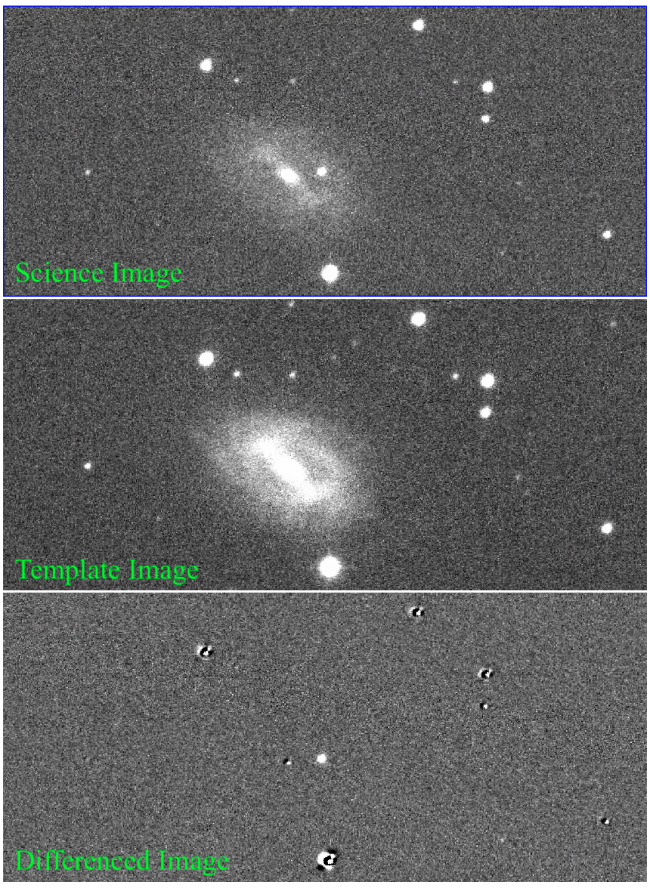

Figure 4. Example image subtraction from DEHVILS for SN 2020kpx in the UKIRT J-band. **Upper**: Image of the SN and host galaxy. Modified Julian Date (MJD): 59000. **Middle**: Image of the host galaxy more than a year past SN peak brightness. MJD: 59466. **Lower**: Subtracted image where the template image has been convolved to fit the science image.

Brout, D., Scolnic, D., Popovic, B., et al., 2022, arXiv e-prints, arXiv:2202.04077, arXiv:2202.04077

Burns, C. R., Parent, E., Phillips, M. M., et al., 2018, ApJ, 869, 1, 56, arXiv:1809.06381

Burns, C. R., Stritzinger, M., Phillips, M. M., et al., 2011, AJ, 141, 1, 19, arXiv:1010.4040

Calcino, J., Davis, T., 2017, JCAP, 2017, 1, 038, arXiv:1610.07695

Carr, A., Davis, T. M., Scolnic, D., et al., 2021, arXiv e-prints, arXiv:2112.01471, arXiv:2112.01471

Carrick, J., Turnbull, S. J., Lavaux, G., Hudson, M. J., 2015, MNRAS, 450, 1, 317, arXiv:1504.04627

Conley, A., Guy, J., Sullivan, M., et al., 2011, ApJS, 192, 1, 1, arXiv:1104.1443

Crook, A. C., Huchra, J. P., Martimbeau, N., Masters, K. L., Jarrett, T., Macri, L. M., 2007, ApJ, 655, 2, 790, arXiv:astro-ph/0610732

Davis, T. M., Hinton, S. R., Howlett, C., Calcino, J., 2019, MNRAS, 490, 2, 2948, arXiv:1907.12639

Freedman, W. L., Madore, B. F., Hatt, D., et al., 2019, ApJ, 882, 1, 34, arXiv:1907.05922

Graziani, R., Courtois, H. M., Lavaux, G., et al., 2019, MNRAS, 488, 4, 5438, arXiv:1901.01818

Guy, J., Sullivan, M., Conley, A., et al., 2010, A&A, 523, A7, arXiv:1010.4743

Harrison, E., 1993, ApJ, 403, 28

Hinton, S., Brout, D., 2020, Journal of Open Source Software, 5, 47, 2122

Hoaglin, D. C., Mosteller, F., (Editor), J. W. T., 2000, Understanding Robust and Exploratory Data Analysis, Wiley-Interscience, 1st edn.

Huchra, J. P., Geller, M. J., 1982, ApJ, 257, 423

Hunter, J. D., 2007, Computing In Science & Engineering, 9, 3, 90

Kelly, P. L., Hicken, M., Burke, D. L., Mand el, K. S., Kirshner, R. P., 2010, ApJ, 715, 2, 743, arXiv:0912.0929

Kenworthy, W. D., Scolnic, D., Riess, A., 2019, ApJ, 875, 2, 145, arXiv:1901.08681

Kessler, R., Becker, A. C., Cinabro, D., et al., 2009, ApJS, 185, 1, 32, arXiv:0908.4274

Kessler, R., Scolnic, D., 2017, ApJ, 836, 1, 56, arXiv:1610.04677

Lambert, T. S., Kraan-Korteweg, R. C., Jarrett, T. H., Macri, L. M., 2020, MNRAS, arXiv:2007.00581

Lampeitl, H., Smith, M., Nichol, R. C., et al., 2010, ApJ, 722, 1, 566, arXiv:1005.4687

Lavaux, G., Hudson, M. J., 2011, MNRAS, 416, 4, 2840, arXiv:1105.6107

Lilow, R., Nusser, A., 2021, MNRAS, 507, 2, 1557, arXiv:2102.07291

Lim, S. H., Mo, H. J., Lu, Y., Wang, H., Yang, X., 2017, MNRAS, 470, 3, 2982, arXiv:1706.02307

Mould, J. R., Huchra, J. P., Freedman, W. L., et al., 2000, ApJ, 529, 2, 786, arXiv:astro-ph/9909260

Neill, J. D., Hudson, M. J., Conley, A., 2007, ApJL, 661, 2, L123, arXiv:0704.1654

Peebles, P. J. E., 1993, Principles of Physical Cosmology

Planck Collaboration, Aghanim, N., Akrami, Y., et al., 2020, A&A, 641, A1, arXiv:1807.06205

Ponder, K. A., Wood-Vasey, W. M., Weyant, A., et al., 2021, ApJ, 923, 2, 197, arXiv:2006.13803

Price-Whelan, A. M., Sipőcz, B. M., Günther, H. M., et al., 2018, AJ, 156, 123

Rahman, W., Trotta, R., Boruah, S. S., Hudson, M. J., van Dyk, D. A., 2021, arXiv e-prints, arXiv:2108.12497, arXiv:2108.12497

Riess, A. G., Casertano, S., Yuan, W., Macri, L. M., Scolnic, D., 2019, ApJ, 876, 1, 85, arXiv:1903.07603

Riess, A. G., Macri, L. M., Hoffmann, S. L., et al., 2016, ApJ, 826, 1, 56, arXiv:1604.01424

Riess, A. G., Yuan, W., Macri, L. M., et al., 2021, arXiv e-prints, arXiv:2112.04510, arXiv:2112.04510

Rigault, M., Copin, Y., Aldering, G., et al., 2013, A&A, 560, A66, arXiv:1309.1182

Said, K., Colless, M., Magoulas, C., Lucey, J. R., Hudson, M. J., 2020, MNRAS, 497, 1, 1275, arXiv:2007.04993

Scolnic, D., Brout, D., Carr, A., et al., 2021, arXiv e-prints, arXiv:2112.03863, arXiv:2112.03863

Scolnic, D. M., Jones, D. O., Rest, A., et al., 2018, ApJ, 859, 2, 101, arXiv:1710.00845

Springob, C. M., Magoulas, C., Colless, M., et al., 2014, MNRAS, 445, 3, 2677, arXiv:1409.6161

Sullivan, M., Conley, A., Howell, D. A., et al., 2010, MNRAS, 406, 2, 782, arXiv:1003.5119

Tripp, R., 1998, A&A, 331, 815

Tully, R. B., 2015, AJ, 149, 5, 171, arXiv:1503.03134

Tully, R. B., Courtois, H. M., Sorce, J. G., 2016, AJ, 152, 2, 50, arXiv:1605.01765

Uddin, S. A., Burns, C. R., Phillips, M. M., et al., 2020, ApJ, 901, 2, 143, arXiv:2006.15164

Van Der Walt, S., Colbert, S. C., Varoquaux, G., 2011, Computing in Science & Engineering, 13, 22, arXiv:1102.1523

Wojtak, R., Davis, T. M., Wiis, J., 2015, JCAP, 2015, 7, 025, arXiv:1504.00718

Wright, A. H., Hildebrandt, H., van den Busch, J. L., et al., 2020, A&A, 640, L14, arXiv:2005.04207